F. You, S. Zheng, T. Pang, L. Zeng,
L. Lei, S. Lin,* J. Zhang, T. Shen,
F. Huang, D. Chen* 2400838

Transparent $Ho^{3+}/Tm^{3+}/Er^{3+}/Yb^{3+}$ Codoped Nano-Glass-Ceramics for Upconversion Head-Up Display

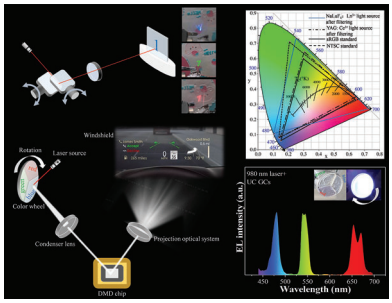

A brand-new NIR laser-driven UC HUD system using nano-glass-ceramics containing lanthanide-doped $NaLuF_4$ nanocrystals is developed. Importantly, two types of unprecedented HUD prototypes based on the developed pure R/G/B UC glass ceramics demonstrate a wide color gamut of 115% NTSC, 163% sRGB, and 156% conventional lighting sources.

LASER & PHOTONICS REVIEWS
www.lpr-journal.org

Transparent $Ho^{3+}/Tm^{3+}/Er^{3+}/Yb^{3+}$ Codoped Nano-Glass-Ceramics for Upconversion Head-Up Display

Fengluan You, Song Zheng, Tao Pang, Lingwei Zeng, Lei Lei, Shisheng Lin, Jinzhe Zhang, Tongjie Shen, Feng Huang, and Daqin Chen**

The commonly used automotive head-up display (HUD) technology is confronted with the problems of poor stability in organic resin counterpart and the unsatisfactory display effect of projection lighting source. To solve these issues, developing state-of-the-art materials and designing new HUD schemes with a wide color gamut is of necessity. Herein, a series of pure red/green/blue (R/G/B) upconverting (UC) nano-glass-ceramics (GCs) containing lanthanide-doped $NaLuF_4$ nanocrystals (NCs) are synthesized in a cost-effective, environment-friendly, and scalable manner, simultaneously achieving high crystallinity (≈45.44%) and high transparency (>80%). Yb^{3+} is chosen as the sensitizer to Tm^{3+} (blue UC)/Ho^{3+} (green UC), due to its large absorption cross section from ground state $^2F_{7/2}$ to excited state $^2F_{5/2}$; meanwhile Er^{3+}, Tm^{3+} co-doped into NCs can obtain pure red UC emission via promoting the population of Er^{3+} red-emitting $^4F_{9/2}$ state. Consequently, the as-prepared materials exhibit high R/G/B color purity of > 80% owing to the energy transfer between different lanthanide ions (Yb^{3+}, Tm^{3+}, Ho^{3+}, and Er^{3+}) upon 980 nm near-infrared (NIR) laser excitation, and possess superior thermal reversibility/water resistivity. Remarkably, two unprecedented HUD prototypes are constructed to demonstrate the application feasibility of developed pure R/G/B UC GCs.

1. Introduction

With the advent of the Internet of Things era, an up-to-date application, automotive HUD, can present important driving information including speed, fuel consumption, tire pressure, and water temperature on the interface horizontally,[1–3] thereby effectively reducing the traffic accident rates and garnering public attention. The first demonstration of applying HUD into automobiles was proposed by the American general motor in 1980s.[4] Thereafter, the validity of HUD was further manifested in some high-end car models by BMW, Audi, Geely et al.[5] Generally, automotive HUD has two subcategories: combiner HUD system and windshield HUD system.[6] The former one is to place an additional combiner (mostly transparent resin class) on the dashboard or light barrier for obtaining image, while the latter is to project directly on the windshield. Nevertheless, the commonly used HUD technology is confronted with the problem of poor stability in organic resin counterpart, i.e., the related materials suffer from severe age and turn yellow upon long-term usage;[5] besides, the corresponding display effect of HUD projection lighting source also needs to be improved. The conventional lighting source, phosphor-converted white light-emitting diodes (pc-wLEDs) based on the "blue chip + $Y_3Al_5O_{12}$: Ce^{3+} (YAG: Ce^{3+})", is not seen as the best selection for display applications, because of its narrow color gamut from filtering its broadband emitting light into R/G/B primary colors.[7,8] Therefore, it is highly desirable

F. You, S. Zheng, S. Lin, J. Zhang, T. Shen, F. Huang, D. Chen
College of Physics and Energy
Fujian Normal University
Fuzhou, Fujian 350117, P. R. China
E-mail: linshisheng@fjnu.edu.cn; dqchen@fjnu.edu.cn

T. Pang
Huzhou Key Laboratory of Materials for Energy Conversion and Storage
College of Science
Huzhou University
Huzhou, Zhejiang 313000, China

L. Zeng
School of Chemistry and Chemical Engineering
Hunan University of Science and Technology
Xiangtan, Hunan 411201, P. R. China

L. Lei
Institute of Optoelectronic Materials and Devices
China Jiliang University
Hangzhou 310018, P. R. China

S. Lin, D. Chen
Fujian Provincial Collaborative Innovation Center for Advanced High-Field Superconducting Materials and Engineering
Fujian Normal University
Fuzhou, Fujian 350117, P. R. China

S. Lin, D. Chen
Fujian Provincial Engineering Technology Research Center of Solar Energy Conversion and Energy Storage
Fujian Normal University
Fuzhou, Fujian 350117, P. R. China

The ORCID identification number(s) for the author(s) of this article can be found under https://doi.org/10.1002/lpor.202400838

DOI: 10.1002/lpor.202400838

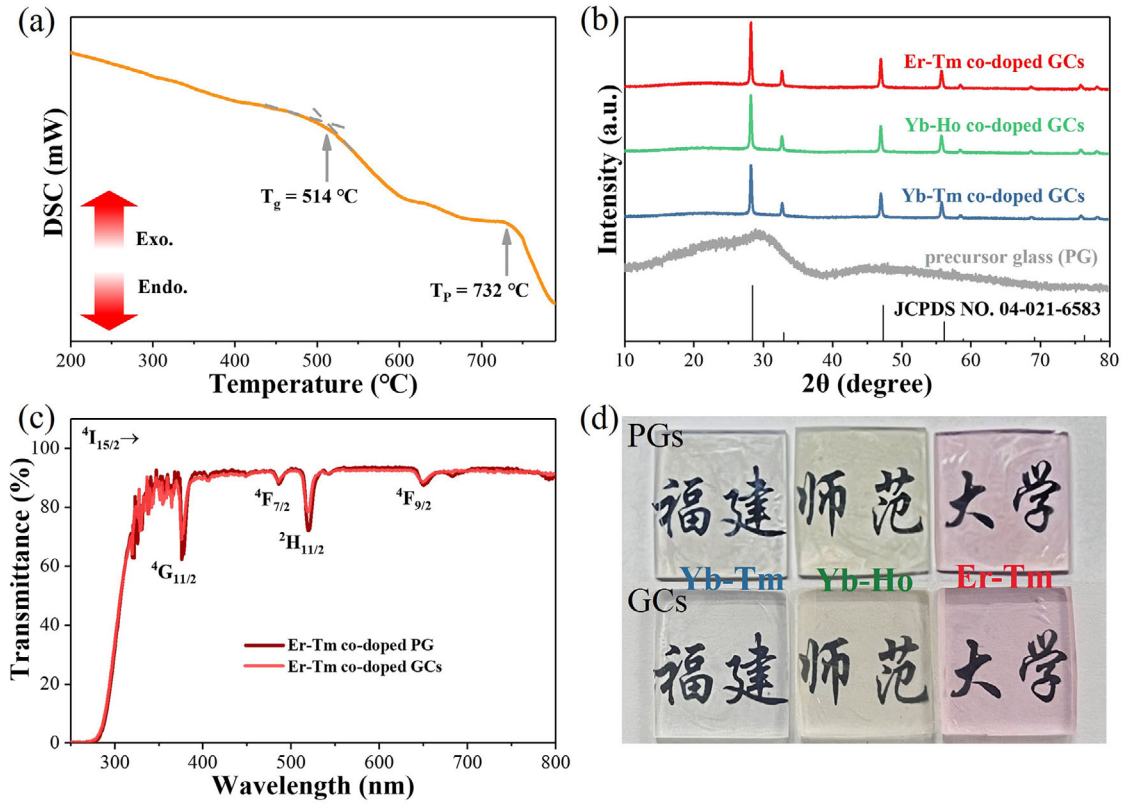

Figure 1. a) DSC curve of precursor glass (PG) recorded at a heating rate of 10 °C min^{-1}. b) XRD patterns of PG and Ln^{3+}-doped GCs. c) Transmission spectra of Er^{3+}-Tm^{3+} co-doped PG and GC. d) The digital photos of the samples under natural light.

to develop new stable materials and new HUD schemes with a wide color gamut to address these issues.

Tm^{3+}/Ho^{3+}/Er^{3+} doped low-phonon hosts (e.g., $NaYF_4$, $BaYF_5$, $CsYb_2F_7$) leverage their distinct energy level transitions to achieve blue/green/red UC luminescence through meticulous regulation of the concentration of doped lanthanide ions and the inclusion of sensitizers like Yb^{3+}.[9–15] Herein, a novel NIR-laser-driven UC HUD is reported for the first time. UC GCs containing highly-ordered lanthanide (Ln^{3+}) doped $NaLuF_4$ NCs, with their combined merits of low phonon energy from fluoride for Ln^{3+} activators and physical/chemical stabilities from robust glass,[16–21] are selected as the color converters. This kind of advanced inorganic nanocomposite highlights tunable R/G/B UC emissions from the ultraviolet (UV) to NIR region with line spectrum by multi-photon absorption mechanism,[22–27] which contributes to elevate the display color gamut to go beyond the 100% NTSC (National Television Standard Committee) standard. The design of UC HUD is realized via two approaches: 1) transparent UC GCs are placed in the driver's view with a 980 nm NIR laser to visualize information; 2) UC GCs act as color converters in a rotating "wheel" with an R/G/B pattern, elaborately coupled with a 980 nm excitation laser and imager module to display a color image on the windshield. Importantly, the balance between high crystallinity (≈45.44%) and high transparency (>80%) of UC GC is leveraged. The optimized transparent R/G/B UC GCs show high color purity (>80%), robustness, and thermal/chemical stability. Importantly, owing to the admirable features, it demonstrates unprecedented HUD scheme with a wide color gamut, where the self-built demo can cover a color gamut of 115% NTSC, 163% sRGB, and 156% conventional lighting source. This work provides innovative thoughts and offers clear guidance on designing HUD, hopefully bringing renaissance of the classical UC oxyfluoride GCs containing lanthanide-doped fluoride NCs.

2. Results and Discussion

A controlled solvent-free thermally-driven approach was applied to in situ precipitate Ln^{3+}-doped fluoride NCs, which avoids unfriendly organic-solvent-assisted preparation procedures, low production, and high cost (Experimental Section in Supporting Information).

The precursor glass (PG) is with stoichiometric composition (in mol%) of $60SiO_2$-$6Al_2O_3$-19NaF-$7Na_2CO_3$-(8-x-y)LuF_3-xTmF_3/HoF_3/ErF_3-yYbF_3/TmF_3. Differential scanning calorimetry (DSC) analysis of PG indicates the glass transition temperature (T_g) of ≈514 °C and one exothermic peak (T_p) of ≈732 °C; correspondingly, the heat-treated condition is set at 700 °C for 2 h to enable in situ nucleation/growth of fluoride NCs in amorphous glass (**Figure 1a**). The controlled glass crystallization is recognized as a burdensome task to leverage the balance between high crystallinity and high transparency.[28,29] Based on X-ray diffraction (XRD) patterns of as-prepared PG and GCs (Figure 1b), the precipitated NCs is ascribed to cubic $NaLuF_4$ (JCPDS No. 04-021-6583) with high crystallinity of 45.44% favor-

Table 1. Experimental (f_{exp}) and theoretical (f_{cal}) oscillation strengths in a unit of 10^{-8} and J–O intensity parameters of Er^{3+} in PG and GC.

Transition	PG		GC	
	f_{exp}	f_{cal}	f_{exp}	f_{cal}
$^4I_{15/2}\rightarrow{}^4G_{11/2}$	757.00	743.48	743.55	704.96
$\rightarrow{}^4F_{7/2}$	329.70	329.76	347.10	347.26
$\rightarrow{}^2H_{11/2}$	407.97	420.64	361.86	397.92
$\rightarrow{}^4F_{9/2}$	236.70	236.61	239.90	239.63
Rms (10^{-7})	1.85		5.28	
Ω_2 (10^{-20} cm^2)	3.12		2.96	
Ω_4 (10^{-20} cm^2)	1.17		1.02	
Ω_6 (10^{-20} cm^2)	3.28		3.47	

able for photonic application. Notably, doping Ln^{3+} ions (Yb^{3+}, Tm^{3+}, Ho^{3+} and Er^{3+}) does not induce any impurities. Meanwhile, the transmittance in visible region is higher than 80% for all the PG and GCs with thickness of 0.5 mm, except for the absorption bands from the distinguished transitions of the Er^{3+} ions from $^4I_{15/2}$ to $^4G_{11/2}$, $^4F_{7/2}$, $^2H_{11/2}$, and $^4F_{9/2}$, respectively (0; Figure S1, Supporting Information). From transmittance spectra, the experimental oscillator strengths were obtained and then the Judd–Ofelt (J-O) intensity parameters Ω_λ ($\lambda = 2, 4, 6$) of Er^{3+} were calculated (**Table 1**). The Judd–Ofelt parameter Ω_2 is associated with short-range coordination chemistry, offering insights into the symmetry, local structure, and covalency of metal-ligand bonds surrounding Ln^{3+}. In contrast, parameters Ω_4 and Ω_6 reflect the degree of orbital overlap in lanthanide-doped glasses and

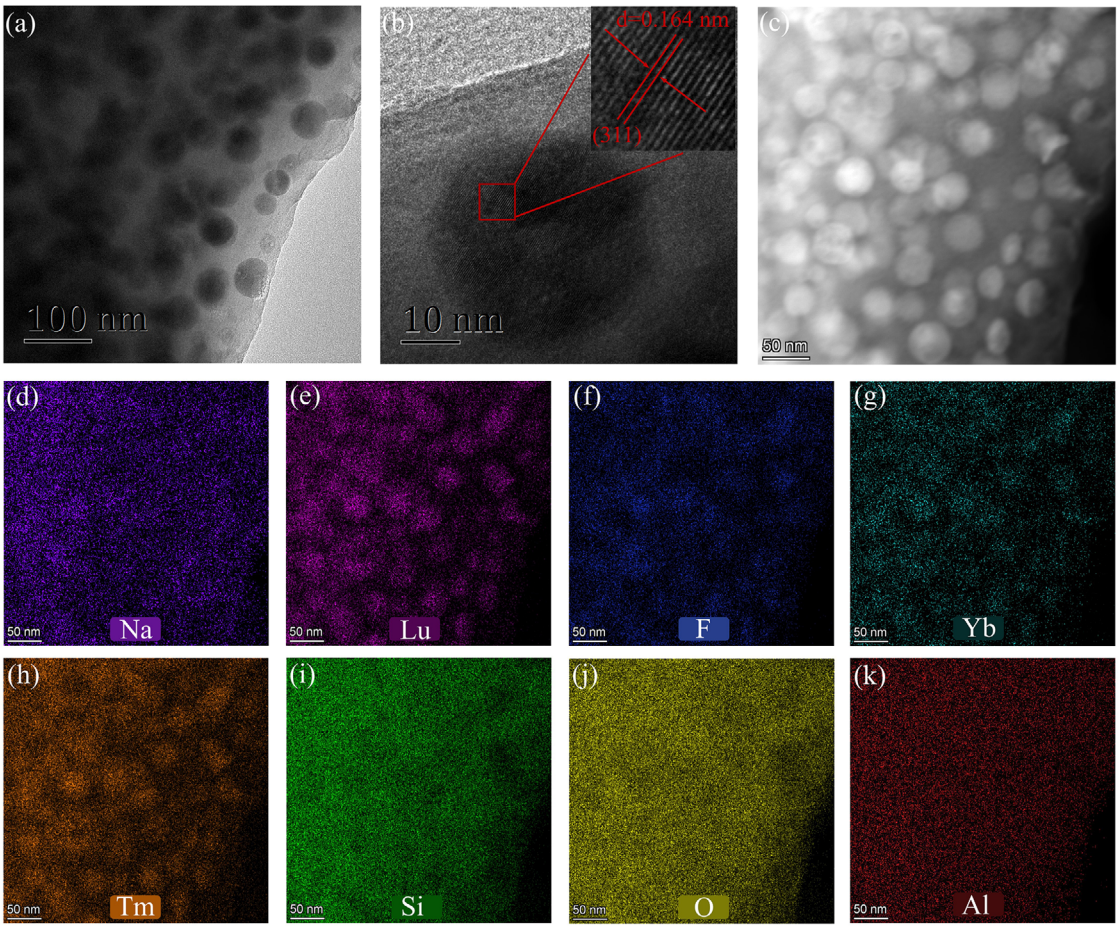

Figure 2. a) TEM image of $NaLuF_4$: Yb-Tm NCs @glass. b) HRTEM image of a typical $NaLuF_4$: Yb-Tm NC inside glass matrix. c) HAADF-STEM image of $NaLuF_4$: Yb-Tm NCs @glass, and related EDS map-scanning of d) Na, e) Lu, f) F, g) Yb, h) Tm, i) Si, j) O, k) Al.

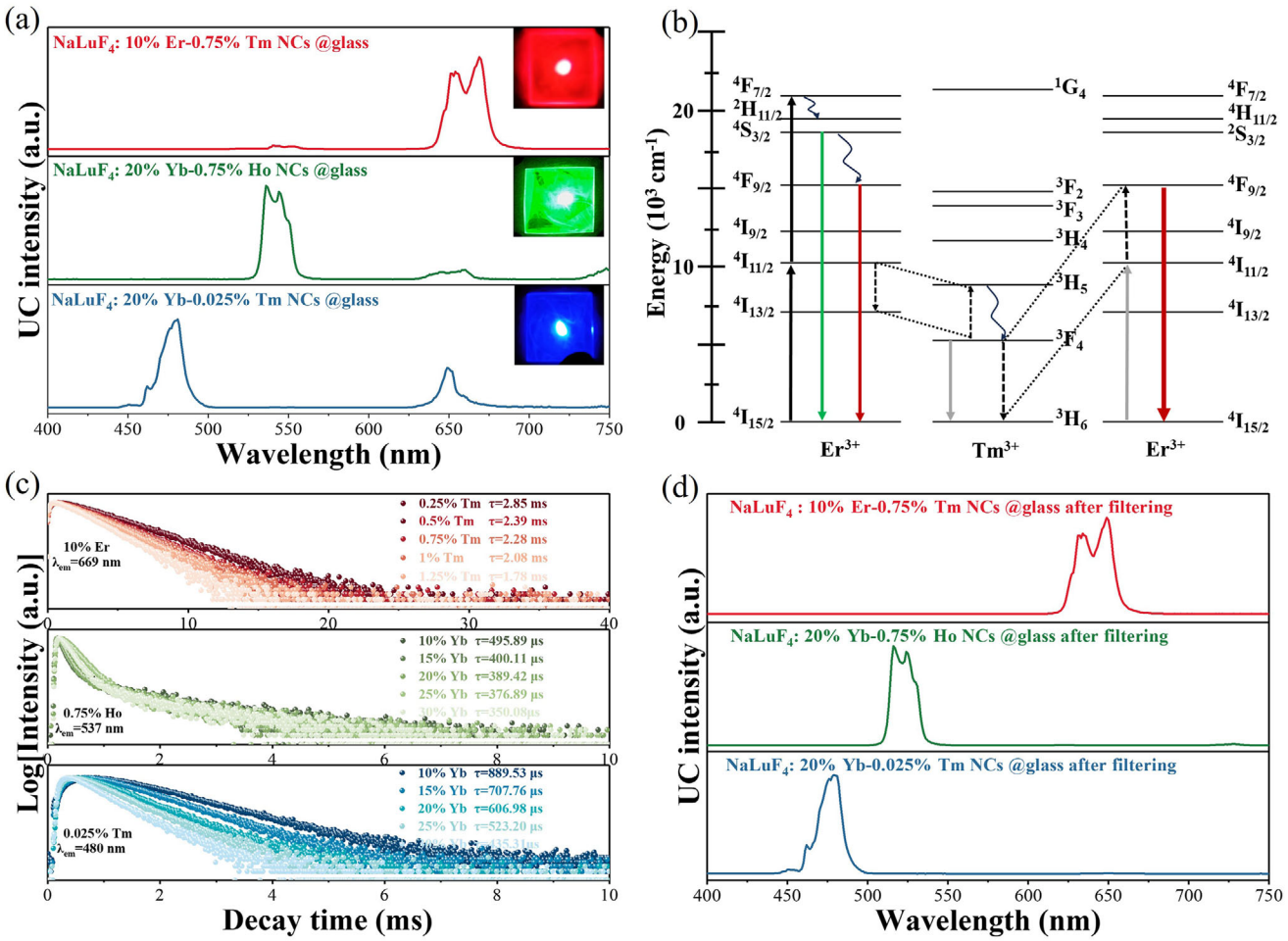

Figure 3. a) UC emission spectra of $NaLuF_4$: 20% Yb-0.025% Tm NCs @glass, $NaLuF_4$: 20% Yb-0.75% Ho NCs @glass and $NaLuF_4$: 10% Er-0.75%Tm NCs @glass under 980 nm NIR laser excitation. Insets show the corresponding photographs of GCs under 980 nm NIR laser excitation. b) Simplified energy level diagram of Er^{3+} and Tm^{3+}. c) The Yb^{3+}/Tm^{3+} concentration-dependent UC decay curves by monitoring 480 nm (Tm^{3+}), 537 nm (Ho^{3+}), and 669 nm (Er^{3+}) emissions, respectively. d) Corresponding UC emission spectra after passing through red, green, and blue filters, respectively.

encompass long-range characteristics such as rigidity, viscosity, and the dielectric constant of the matrix. Comparisons of Ω_4 and Ω_6 across glasses with varying compositions can elucidate differences in their amorphous structures, which is influenced by network formers (such as SiO_2, B_2O_3, and P_2O_5) and modifiers (such as Na_2O and CaO). For PG and GC of the same composition, the parameter Ω_2 is typically assessed to detect any changes in the environment of Ln^{3+}, as it is more sensitive to local structural alterations. The variation of Ln^{3+} dopants from amorphous oxide environment to fluoride environment can reduce the value of Ω_2.[30] Similarly, it is shown that the value of Ω_2 in GCs is smaller than in PG, indicating that Er^{3+} ions enter $NaLuF_4$ crystalline environment.

Transmission electron microscope (TEM) image of typical $NaLuF_4$: Yb-Tm NCs @glass shows the monodispersed particles precipitated in glass matrix with the size of ≈38.5 nm (**Figure 2a**; Figure S2, Supporting Information). High-resolution TEM (HRTEM) observation of an individual nanoparticle discloses well-resolved lattice fringes with a measured interplanar spacing of 0.164 nm, corresponding to the theoretical value (0.1637 nm) of (311) facet from cubic $NaLuF_4$ (Figure 2b).[31] High-angle annular dark-field scanning TEM (HAADF-STEM) image clearly distinguishes the Z-contrast between $NaLuF_4$ NCs (bright) and aluminosilicate glass matrix (dark), because the large difference in atomic number: Lu (Z = 71) enriched in the NCs (versus Al/Si, Z = 14/13) can scatter more electrons (Figure 2c). In the energy dispersive spectroscopy (EDS) map-scanning analyses, Na, Lu, F, Yb and Tm elements were observed in the particle region, demonstrating its chemical composition; whereas Si and Al signals can be detected in the glass matrix (Figure 2d–k). Evidently, the self-limited growth of NCs in the aluminosilicate glass with strong network structure enables the fabrication of highly-ordered $NaLuF_4$ NCs embedded glass.

In order to achieve better HUD color quality under the excitation of 980 nm near-infrared (NIR) laser, the appropriate UC GCs containing Ln^{3+}-doped $NaLuF_4$ should be fabricated to obtain pure R/G/B UC. As such, Yb^{3+} was chosen as the sensitizer for absorbing infrared radiation and non-radiatively transferring excitation to Tm^{3+} (blue UC)/Ho^{3+} (green UC), due to its large absorption cross section from ground state $^2F_{7/2}$ to excited

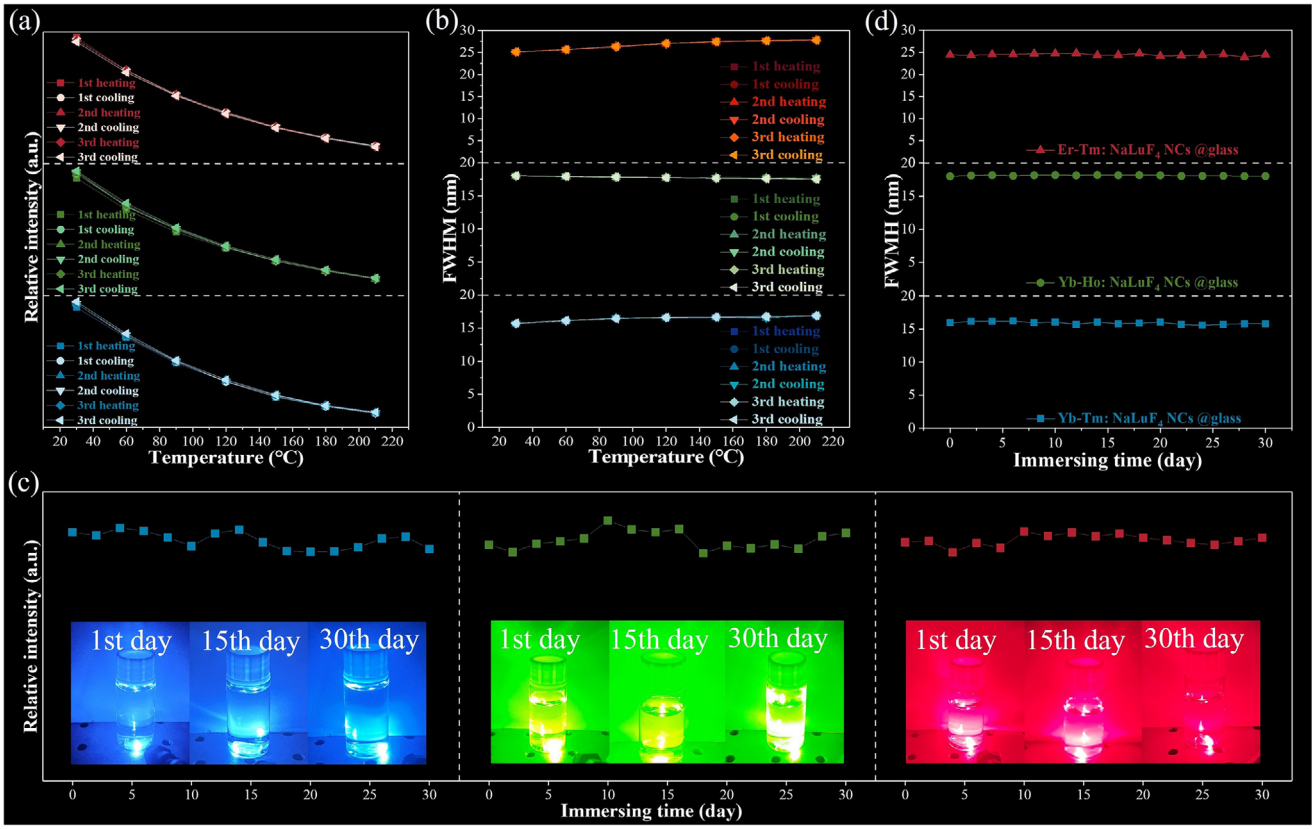

Figure 4. a) Relative PL intensity and b) FWHM of $NaLuF_4$: Yb-Tm NCs @glass, $NaLuF_4$: Yb-Ho NCs @glass and $NaLuF_4$: Er-Tm NCs @glass undergoing three 30–210 °C heating/cooling cycles. c) Relative PL intensity and d) FWHM for three typical GCs immersed in water for 30 days. Inset of c) reveals the corresponding luminescent photos excited by 980 nm NIR laser.

state $^2F_{5/2}$ (Figures S3 and S4, Supporting Information);[32,33] meanwhile Er^{3+}, Tm^{3+} co-doped into NCs can obtain pure red UC emission via enhancing the $^4F_{9/2} \rightarrow {}^4I_{15/2}$ (~669 nm) transition of Er^{3+} (**Figure 3**a,b), originating from the following cross-relaxations (CR) and energy transfer UC process (ETU):

$$\mathrm{CR}: \mathrm{Er}^{3+}{:}^4\mathrm{I}_{11/2} + \mathrm{Tm}^{3+}{:}^3\mathrm{F}_4 \rightarrow \mathrm{Er}^{3+}{:}^4\mathrm{I}_{13/2} + \mathrm{Tm}^{3+}{:}^3\mathrm{H}_5 \quad (1)$$

$$\mathrm{ETU}: \mathrm{Er}^{3+}{:}^4\mathrm{F}_{9/2} + \mathrm{Tm}^{3+}{:}^3\mathrm{H}_6 \rightarrow \mathrm{Er}^{3+}{:}^4\mathrm{I}_{11/2} + \mathrm{Tm}^{3+}{:}^3\mathrm{F}_4 \quad (2)$$

In this regard, Er^{3+} ions in the $^4I_{15/2}$ ground state are pumped to the $^4F_{7/2}$ excited state through successive absorption of 980 nm NIR photons. Subsequently, non-radiative multi-photon relaxations populate the green-emitting $^2H_{11/2}/^4S_{3/2}$ and red-emitting $^4F_{9/2}$ states. As Tm^{3+} is co-doped into NCs, the CR process occurs. However, there is a large energy gap between the Tm^{3+} $^3F_4$ excited state and $^3H_6$ ground state, essentially prohibiting nonradiative multiphonon relaxation (MPR).[34] The electrons will store in the Tm^{3+} $^3F_4$ excited state and promote the population of Er^{3+} red-emitting $^4F_{9/2}$ state via ETU.

Next, taking overall consideration of emission intensity, peak profile, and color purity, the Yb^{3+}, Tm^{3+}, Ho^{3+}, and Er^{3+} concentrations are optimized upon 980 nm NIR laser excitation, thereby making the final color purity of R/G/B UC achieve 84.08%, 84.57%, and 80.60%, respectively (Figures S5–S8, Supporting Information). Probing the variation of Ln^{3+} doping content-dependent UC luminescent decay curves, the energy transfers between designed sensitizers and activators were clarified: as the contents of Yb^{3+} and Tm^{3+} (sensitizers) increase, the lifetime continuously declines for all samples due to the increased non-radiative transition caused by shorter distances between Ln^{3+} (Figure 3c). To be noted, a normal frame rate of 60 Hz implies that the display refreshes every 16.67 ms. If the decay time of the UC material exceeds this period, it could result in motion blur or ghosting effects, as the UC material may not return to its ground state before the next frame is rendered. Fortunately, the decay times of the developed $NaLuF_4$: Yb-Tm NCs @glass, $NaLuF_4$: Yb-Ho NCs @glass, and $NaLuF_4$: Er-Tm NCs @glass are ≈2.28, 0.389, and 0.607 ms, respectively, which do not significantly impact the temporal response of HUD displays operating at a standard frame rate of 60 Hz. Moreover, the line UC spectrum of developed pure R/G/B UC GCs containing Ln^{3+}-doped $NaLuF_4$ match the commercial filters well, which can help decrease the luminance loss upon filtering (Figure 3d; Figures S9–S11, Supporting Information).

Furthermore, pumping-power-dependent UC emission spectra were measured under 980 nm NIR laser excitation. The slope of the linear fitting for the blue emission at 480 nm (Tm^{3+}: $^1G_4 \rightarrow {}^3H_6$) of $NaLuF_4$: Yb-Tm NCs @glass is close to 3, indicating that three photons are involved in its blue upconversion emission (Figure S12, Supporting Information). In contrast, the slopes for the green upconversion emission of $NaLuF_4$: Yb-Ho NCs

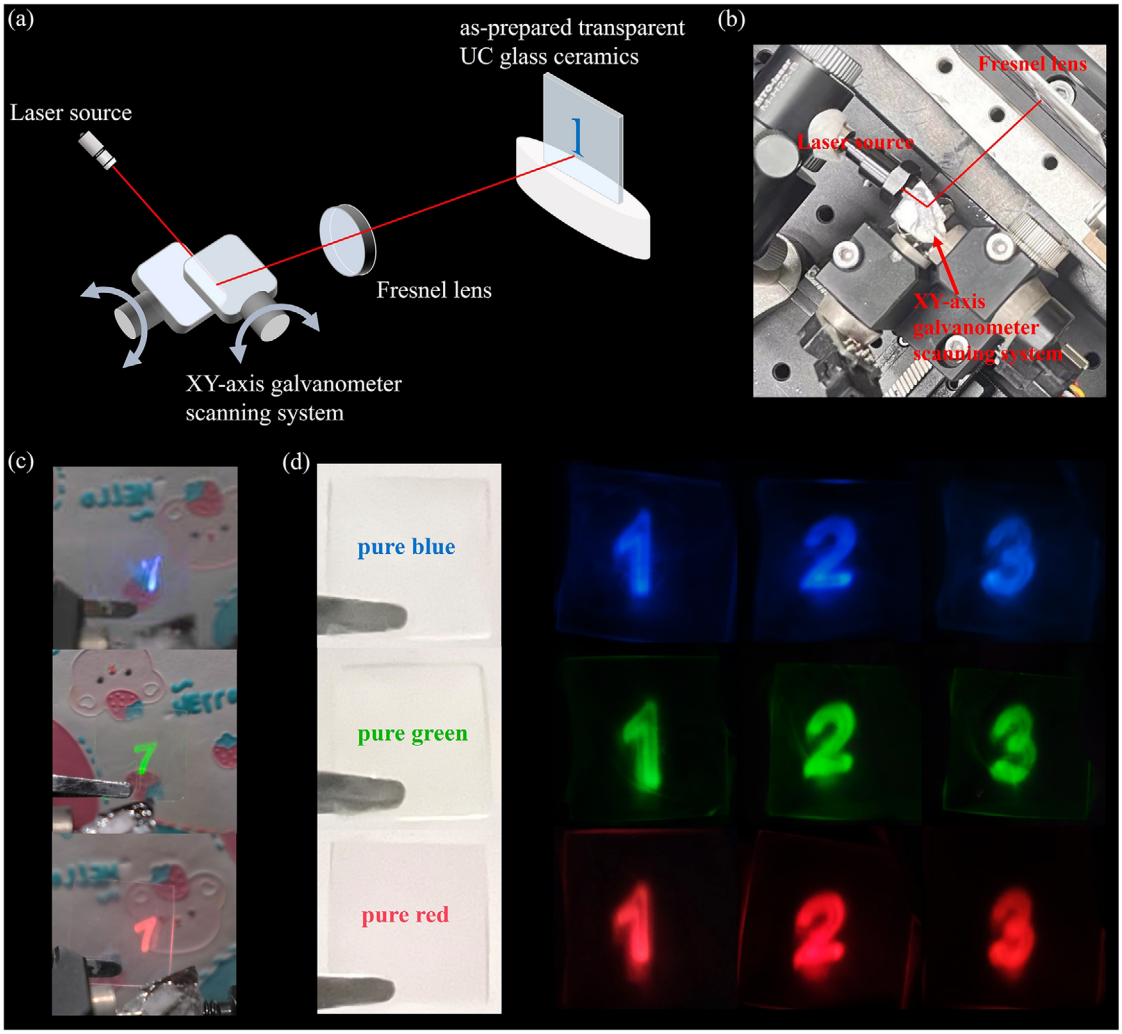

Figure 5. a) Schematic illustration of the proposed combiner HUD system and b) corresponding photograph. Digital photographs of designed number patterns in pure R/G/B UC GCs under c) sunlight and d) dark environment.

@glass and the red upconversion emission of $NaLuF_4$: Er-Tm NCs @glass are near 2, revealing that two photons are required to populate the green-emitting $^5F_4$ state of Ho^{3+} and the red-emitting $^4F_{9/2}$ state of Er^{3+}, respectively (Figures S13 and S14, Supporting Information). Under 980 nm NIR laser excitation with a pumping power of 33.4 W cm^{-2}, the conversion efficiencies (UCQY) are 0.007%, 0.009%, and 0.004% for optimized $NaLuF_4$: Yb-Tm NCs @glass, $NaLuF_4$: Yb-Ho NCs @glass, and $NaLuF_4$: Er-Tm NCs @glass, respectively (Figures S15–S17, Supporting Information). In addition, the absorption spectra of the optimized $NaLuF_4$: Yb-Tm NCs @glass, $NaLuF_4$: Yb-Ho NCs @glass, and $NaLuF_4$: Er-Tm NCs @glass exhibit absorption coefficients at the 980 nm waveband of ≈1.13, 1.21, and 0.46 cm^{-1}, respectively (Figures S18–S20, Supporting Information).

Furthermore, pure R/G/B UC lanthanide-doped $NaLuF_4$: NCs @glass were subjected to a series of stability tests. All the samples exhibit superior thermal reversibility: their luminescence intensity can be recovered even undergoing three 30–210 °C heating/cooling cycles, benefiting from the rigid glass matrix preventing ionic migration to cope with thermal shock (**Figure** 4a; Figures S21–S23, Supporting Information). Moreover, Yb-Tm: $NaLuF_4$: NCs @glass (blue UC), Yb-Ho: $NaLuF_4$: NCs @glass (green UC), and Er-Tm: $NaLuF_4$: NCs @glass (red UC) show ultra-narrow UC luminescence spectra with full-width at half-maximum (FWHM) of ≈16, ≈18, and ≈26 nm, respectively, catering to display application. As shown in Figure 4b, there is no change of FWHM when elevating the temperature, indicating that no structural variation would occur unless the T_g is reached. To be noted, considering T_g, the used aluminosilicate glass (T_g≈500 °C) obviously exhibits superior physical stability to resin class (T_g≈100 °C),[35] which can well address the poor stability in traditional organic resin matrix in the field of HUD system.

The incorporation of lanthanide-doped $NaLuF_4$ NCs in glass also endows the composite material with superior resistivity to water over a long period. Under being immersed in water for 30 days, UC luminescence of $NaLuF_4$: Yb-Tm NCs @glass, $NaLuF_4$: Yb-Ho NCs @glass, and $NaLuF_4$: Er-Tm NCs @glass all can still retain the initial intensity without FWHM change, thanks to the encapsulation of water-impermeable glass matrix (Figure 4c,d).

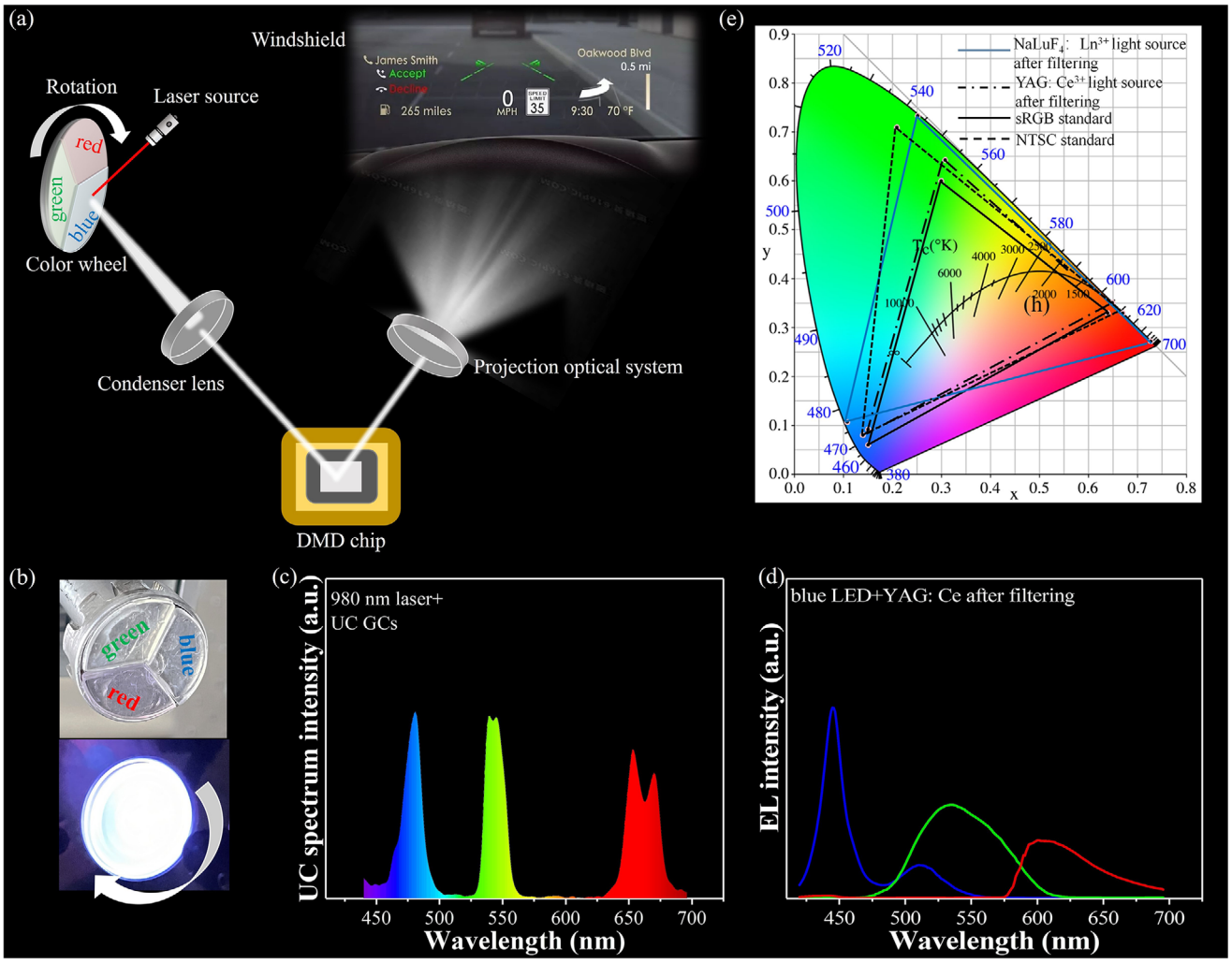

Figure 6. a) Schematic diagram of the supposed windshield HUD system. b) Digital photographs of "wheel" with "pure R/G/B patterned package design". c) UC spectrum of prototype device. d) EL spectrum of conventional lighting source after filtering. e) Color gamut of the prototype device (blue solid triangle), conventional lighting source (black dash-dot triangle), sRGB standard (black solid triangle), and NTSC 1953 standard (black dash triangle).

The nanostructure of lanthanide-doped $NaLuF_4$: NCs @glass makes the nanoscale displayed resolution possible and enables the elevation in color gamut when applied to HUD. A further proof-of-concept experiment on two types of HUD system was performed on the transparent GCs with pure R/G/B UC for the first time. The first method is achieved by real-time programming of the *xy*-axis galvanometer system to vibrate, followed by employing a 980 nm NIR laser to pump the as-prepared GCs to make items visualized (**Figure** 5a,b). The luminous flux (LF) of the prototype device is rigorously assessed under 980 nm NIR laser excitation at a pumping power of 100 W cm^{-2}, which demonstrated a LF of 33.2 lm for blue UC GC, 36.6 lm for green UC GC, and 27.6 lm for red UC GC, ensuring the display pattern's visibility under daylight conditions (Figure 5c). One can observe the number patterns with different color in lanthanide-doped $NaLuF_4$: NCs @glass, which would not disturb the observation of drivers (Figure 5c,d; Movie S1, Supporting Information). We evaluated the theoretical resolution of the developed HUD system. Ideally, utilizing the developed pure R/G/B UC lanthanide-doped $NaLuF_4$: NCs @glass, with a 980 nm near-infrared laser as the excitation source and a Fresnel lens with a numerical aperture (NA) of 0.85 for display, the resolution limits can be determined using various empirical methods: Abbe resolution limit: $\triangle r = 0.5\lambda_0/\mathrm{NA} = 576$ nm; Rayleigh resolution limit: $\triangle r = 0.61\lambda_0/\mathrm{NA} = 703$ nm; Sparrow resolution limit: $\triangle r = 0.47\lambda_0/\mathrm{NA} = 542$ nm. Assuming that both the pixel points and the screen are square in shape, the corresponding pixel areas are $\approx 3.32 \times 10^{-9}$ cm^2, 4.94×10^{-9} cm^2, or 2.94×10^{-9} cm^2, respectively. Consequently, the number of pixel points per square centimeter of the screen would be 300 million, 200 million, or 340 million, respectively, enabling a high-resolution display on the screen.

On the other hand, it is schematically illustrated the supposed prototype windshield HUD system for displaying color images on the windshield, composing of NIR laser, R/G/B UC GCs-based rotating "wheel" with "pure R/G/B patterned

package design", digital micromirror device (DMD) chip and various condensing/projection lenses (**Figure 6a**). The "wheel" functions as color converters to be elaborately coupled with a 980 nm excitation laser and imager module (Figure 6b). The corresponding UC spectrum of the prototype device (at a rotating speed of 4500 rpm) is presented in Figure 6c, showing isolated RGB emissive components. By reason of its broadband spectra, the color gamut of the conventional lighting source ("blue chip + YAG: Ce^{3+}" pc-wLEDs) is entirely determined by the commercial color filters, and particularly, the green emissive component cannot be completely filtered via the blue commercial color filters (Figure 6d). As expected, the present system covers a triangle color range of 115% NTSC, 163% sRGB, and 156% "blue chip + YAG: Ce^{3+}" pc-wLEDs (Figure 6e), illustrating its promising application in HUD.

3. Conclusion

In summary, we have developed pure R/G/B UC oxyfluoride GCs containing lanthanide-doped fluoride NCs (Er-Tm, Yb-Ho, and Yb-Tm co-doped $NaLuF_4$: NCs @glass) with high color purity (>80%) and proposed two types of novel conceivement to achieve HUD system based on them for the first time. The controlled glass crystallization enables highly-ordered nanostructure, while the self-limited growth of $NaLuF_4$: NCs in a viscous environment helps to resolve the contradiction between high crystallinity and high transparency. In this case, the as-prepared transparent UC GCs exhibit superior thermal reversibility and water resistance thanks to the protection of a robust glass network. Furthermore, demonstration experiments evaluate the application feasibility of this material for HUD for the first time. The designed different-color patterns can be observed in lanthanide-doped $NaLuF_4$: NCs @glass, without disturbing the drivers' observation. Moreover, the present system can cover a color gamut of 115% NTSC, 163% sRGB, and 156% conventional lighting source, which will undoubtedly facilitate the development of HUD technology.

Supporting Information

Supporting Information is available from the Wiley Online Library or from the author.

Acknowledgements

This research was supported by National Natural Science Foundation of China (52272141, 51972060, 12074068, 52102159, 22103013 and 12304442), and Natural Science Foundation of Fujian Province (2022J05091, 2020J02017, 2021J06021, 2021J01190, 2020J01931 and 2020H0026).

Conflict of Interest

The authors declare no conflict of interest.

Data Availability Statement

The data that support the findings of this study are available from the corresponding author upon reasonable request.

Keywords

display, glass ceramics, lanthanide, luminescent materials, upconversion

Received: June 6, 2024
Revised: July 26, 2024
Published online:

[1] H. Guo, F. Zhao, W. Wang, X. Jiang, *Adv. Mech. Eng.* **2014**, *6*, 380647.
[2] J. Lee, J. Koo, J. Park, M.-C. Lee, in *Proc. 2021 International Conference on Information and Communication Technology Convergence (ICTC)*, IEEE, jeju island **2021**, 701.
[3] Y. Pang, Y. Su, T. Chen, Z. Wang, G. Lv, Q. Feng, in *Proc. 2022 Holography, Diffractive Optics, and Applications XII*, SPIE, Asia **2022**, 311.
[4] V. Milanovic, A. Kasturi, V. Hachtel, in *Proc. 2022 MOEMS and Miniaturized Systems XIV*, SPIE, San Francisco **2015**, *93750*, 43.
[5] L. Wang, B. Chen, C. Yu, W. Ma, in *Proc. 2019 The 19th COTA International conference of Transportation Professionals*, CICTP, Nanjing **2019**, 568.
[6] Á. Sulyok, P. Koppa, A. Barócsi, *Opt. Eng.* **2021**, *60*, 065101.
[7] S. Chen, J. Lin, J. Huang, T. Pang, Q. Ye, Y. Zheng, X. Li, Y. Yu, B. Zhuang, D. Chen, *Adv. Funct. Mater.* **2024**, *34*, 2309293.
[8] S. Liao, S. Jin, T. Pang, S. Lin, Y. Zheng, R. Chen, G. Xi, X. Li, B. Zhuang, F. Huang, D. Chen, *Adv. Funct. Mater.* **2024**, *34*, 2307761.
[9] S. Zeng, G. Ren, C. Xu, *J. Alloys Compd.* **2011**, *509*, 2540.
[10] X. P. Chen, W. J. Zhang, Q. Y. Zhang, *Phys Rev B Condens. Matter.* **2011**, *406*, 1248.
[11] T. Grzyb, S. Balabhadra, D. Przybylska, M. Węcławiak, *J. Alloys Compd.* **2015**, *649*, 606.
[12] L. Huang, L. Wang, X. Xue, D. Zhao, G. Qin, W. Qin, *J. Nanosci. Nanotechnol.* **2011**, *11*, 9498.
[13] W. Huang, M. Ding, H. Huang, C. Jiang, Y. Song, Y. Ni, C. Lu, Z. Xu, *Mater. Res. Bull.* **2013**, *48*, 300.
[14] C. Zhang, P. A. Ma, C. Li, G. Li, S. Huang, D. Yang, M. Shang, X. Kang, J. Lin, *J. Mater. Chem.* **2011**, *21*, 717.
[15] J. Zhu, S. Wang, Z. Yang, S. Liao, J. Lin, H. Yao, F. Huang, Y. Zheng, D. Chen, *Nanoscale* **2022**, *14*, 3407.
[16] P. Li, X. Xu, J. Zhao, P. Awasthi, X. Qiao, J. Du, X. Fan, G. Qian, *J. Rare Earths.* **2022**, *40*, 169.
[17] C. Lin, C. Bocker, C. Rüssel, *Nano Lett.* **2015**, *15*, 6764.
[18] S. Wang, C. Hua, L. Wang, C. Wang, L. Liu, J. Ren, J. Zhang, *Adv. Opt. Mater.* **2024**, *12*, 2302086.
[19] S. Wang, J. Lin, Y. He, J. Chen, C. Yang, F. Huang, D. Chen, *Chem. Eng. J.* **2020**, *394*, 124889.
[20] D. Chen, Z. Wan, Y. Zhou, P. Huang, X. Zhou, Y. Yu, J. Zhong, M. Ding, Z. Ji, *J. Eur. Ceram. Soc.* **2016**, *36*, 679.
[21] S. Wang, J. Zhu, Y. He, Z. Li, J. Lin, S. Liao, F. Huang, P. Huang, Y. Zheng, X. Li, D. Chen, *Laser Photonics Rev.* **2022**, *16*, 2200039.
[22] Y. Cheng, Y. Gao, H. Lin, F. Huang, Y. Wang, *J. Mater. Chem. C* **2018**, *6*, 7462.
[23] F. Wang, X. Liu, *Chem. Soc. Rev.* **2009**, *38*, 976.
[24] B. Zhou, B. Shi, D. Jin, X. Liu, *Nat. Nanotechnol.* **2015**, *10*, 924.
[25] D. Chen, Y. Wang, F. Bao, Y. Yu, *J. Appl. Phys.* **2007**, *101*, 113511.
[26] D. Chen, Y. Wang, Y. Yu, P. Huang, *Appl. Phys. Lett.* **2007**, *91*, 051920.
[27] F. Hu, J. Zhang, O. Giraldo, W. Song, R. Wei, M. Yin, H. Guo, *J. Lumin.* **2018**, *201*, 493.
[28] C. Luo, Y. Jing, Z. Hua, Z. Sui, C. Wang, P. Hu, L. Zheng, S. Qian, L. Yang, X. Sun, G. Tang, H. Cai, Y. Zhu, H. Ban, J. Han, Z. Wang, X. Qiao, J. Ren, J. Zhang, *ACS Appl. Mater. Interfaces* **2023**, *15*, 46226.
[29] J. Ren, X. Lu, C. Lin, R. K. Jain, *Opt. Express* **2020**, *28*, 21522.
[30] L. Zhang, H. Lin, X. Xiang, Y. Cheng, C. Hua, C. Wang, S. Lin, J. Xu, Y. Wang, *J. Eur. Ceram. Soc.* **2019**, *39*, 2155.

[31] Q. Liu, P. Ran, W. Chen, N. Shi, W. Zhang, X. Qiao, T. Jiang, Y. Yang, J. Ren, Z. Wang, G. Qian, X. Fan, *Adv. Sci.* **2023**, *10*, 2304889.
[32] X. Cui, Y. Cheng, H. Lin, F. Huang, Q. Wu, Y. Wang, *Nanoscale* **2017**, *9*, 13794.
[33] S. Chen, W. Song, J. Cao, F. Hu, H. Guo, *J. Alloys Compd.* **2020**, *825*, 154011.
[34] E. M. Chan, G. Han, J. D. Goldberg, D. J. Gargas, A. D. Ostrowski, P. J. Schuck, B. E. Cohen, D. J. Milliron, *Nano Lett.* **2012**, *12*, 3839.
[35] H. Teng, K. Koike, D. Zhou, Z. Satoh, Y. Koike, Y. Okamoto, *J. Polym. Sci. A. Polym. Chem.* **2009**, *47*, 315.